HETEROCYCLES, Vol. 106, No. 6, 2023, pp. 1047 - 1063. © 2023 The Japan Institute of Heterocyclic Chemistry
Received, 29th March, 2023, Accepted, 21st April, 2023, Published online, 25th April, 2023
DOI: 10.3987/COM-23-14851

DESIGN, SYNTHESIS, AND MOLECULAR DOCKING STUDIES OF CHROMAN-4-ONE LINKED THIOSEMICARBAZIDE DERIVATIVES AS INHIBITORS OF KATG AND ANTI-*MYCOBACTERIUM TUBERCULOSIS* AGENTS

Lei Wang, Hong-Mei Dong, Xin Zhao, and Zai-Chang Yang*

College of Pharmacy, Guizhou University, Guiyang 550025, PR China. E-mail: Zai-Chang Yang：yangzaichangzm@163.com (Zai-Chang Yang)

Abstract – Twenty compounds were designed as ligands for molecular docking with *Mtb* KatG, and 13 compounds with high scoring values were selected for synthesis. *In vitro* antimicrobial susceptibility tests have shown that all the 13 compounds have anti-*Mtb* activity (MIC = 1-32 μg/mL). Among the 13 compounds, compound **4g** showed the strongest anti-*Mtb* activity with an MIC of 1 μg/mL. Therefore, the mechanism of action of compound **4g** was preliminarily investigated by molecular docking, enzyme inhibition test, ROS assay, and time-killing curve. The results indicated that the anti-*Mycobacterium tuberculosis* effect of compound **4g** may be related to its inhibition of KatG enzyme. In summary, this study provides a new idea for the development of novel anti-*Mtb* drugs.

Tuberculosis remains one of the most lethal infectious diseases in the world, and *Mycobacterium tuberculosis* (*Mtb*) is the etiological agent responsible for the disease.[1] According to the Global Tuberculosis Report 2022 of World Health Organization (WHO), the global incidence of tuberculosis is estimated to be 10.6 million, with 1.6 million deaths attributed to the disease.[2] Additionally, the burden of drug-resistant tuberculosis (DR-TB) has increased between 2020 and 2021, with an estimated 450,000 cases of rifampicin-resistant tuberculosis (RR-TB) in 2021, of which approximately 78% were classified as multidrug-resistant tuberculosis (MDR-TB).[3] The treatment of DR-TB is prolonged, costly, and challenging, thus highlighting the urgent need for anti-tuberculosis drugs with novel mechanisms of action.

Chroman-4-one (Figure 1, **a**) belongs to the class of heterocyclic compounds, and this unique scaffold is

present in both natural and synthetic small molecules.[4] As reported in the literature, derivatives of chroman-4-one exhibit diverse biological activities, including anti-tuberculosis, anti-cancer, anti-bacterial, and anti-HIV properties.[5] Thus, chroman-4-one is a pharmacophore with multiple biological activities. Thiosemicarbazide (Figure 1, **b**) is also a pharmacophore with broad biological activities, and its derivatives exhibit anti-tuberculosis, anti-cancer, anti-bacterial, anti-viral, anti-fungal, and anti-parasitic activities.[6] Thiacetazone, one of the thiosemicarbazide derivatives, has demonstrated anti-tuberculosis activity with a minimum inhibitory concentration (MIC) against *Mtb* ranging from 0.1 to 0.5 μg/mL.[7]

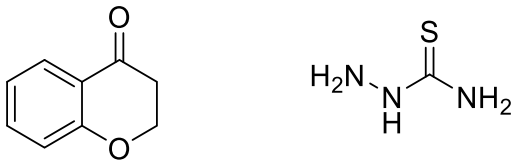

a **b**

Figure 1. a and **b** showed chroman-4-one and thiosemicarbazide, respectively

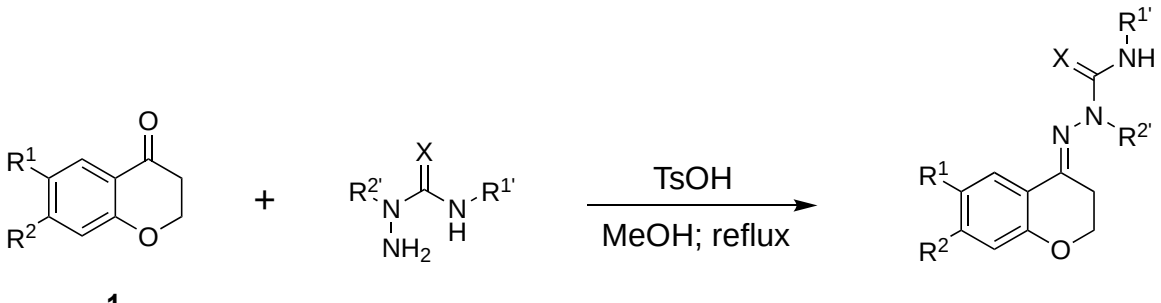

1 **2**

X = O 3a-e
X = S 4f-m

Compound	R^1	R^2	$R^{1'}$	$R^{2'}$
3a	H	Br	Ph	H
3b	H	H	Ph	H
3c	F	H	Ph	H
3d	Cl	H	Ph	H
3e	Me	H	Ph	H
4f	Br	H	H	H
4g	H	Br	H	H
4h	H	H	H	H
4i	F	H	H	H
4j	Cl	H	H	H
4k	Me	H	H	H
4l	OH	H	H	H
4m	Br	H	H	Me

Scheme 1. Synthetic route of 13 compounds

Reactive oxygen species (ROS) are metabolic by-products of *Mtb*. However, when ROS production reaches high levels it can damage *Mtb* macromolecules such as DNA, RNA, lipid molecules, and proteins, which can lead to *Mtb* death. KatG enzyme is a catalase-peroxidase of *Mtb*, which exhibits high catalase activity and peroxidase activity with various substrates. *Mtb* can decompose H_2O_2 by KatG, which reduces the amount of intracellular ROS and enables the intracellular ROS of *Mtb* to be maintained at a reasonable level.[8] In our previous work, a series of compounds with anti-*Mtb* activity were synthesized by combining the quinoline ring with thiosemicarbazone, and their mechanism of action may be related to the inhibition of *Mtb* KatG.[9] Based on this finding, in the present study we designed 20 compounds by collocating chroman-4-one and thiosemicarbazide derivatives. Using Discovery Studio software, these compounds were molecularly docked to *Mtb* KatG. Based on the results of molecular docking, 13 compounds with high affinity to KatG were synthesized. The anti-*Mtb* activity of these compounds was evaluated, and the mechanism of action of compound **4g** was initially explored.

Molecular docking

The results of molecular docking showed that 13 of the 20 compounds designed had relatively high affinity to *Mtb* KatG (Figure S1). Therefore, we assumed that these 13 compounds have anti-*Mtb* activity, and subsequently synthesized these compounds and evaluated their anti-*Mtb* activity. As shown in Figure S1, the molecular docking scores of the other 7 compounds with KatG were low (86.4-94.4), so they were not synthesized.

Chemical synthesis

Total of 13 compounds were synthesized in yields ranging from 60-99% as shown in Scheme 1. The synthesized compounds, all without hydrogen on N, should be the more stable *E* conformation products. These compounds were synthesized by simple methods and the products were easily purified, thus the compounds were not expensive. Since TB is predominantly prevalent among poor populations in developing countries, patients will have difficulty affording treatment if the drugs are expensive, which may result in death due to lack of access to medication. Therefore, it is generally accepted that drugs for the treatment of TB should be inexpensive. The current study raises the possibility of developing a low-cost anti-*Mtb* drug.

Antibacterial activity and SAR analysis

Table 1 shows that all the 13 compounds synthesized have anti-*Mtb* activity. It indicates that the idea of designing anti-*Mtb* molecules using KatG as a target is feasible. The compounds were ranked in order of their antimicrobial activity from strong to weak, and it was seen that the most active compound was compound **4g** with an MIC value of 1 μg/mL against *Mtb*. The results of molecular docking scoring showed that all five compounds (**3a**-**e**) had higher scores than the others, but the *in vitro* anti-*Mtb* results

showed that these five compounds had weaker effects than the others.

This interesting result suggests that predicting the activity of a molecule should take into account the mode the molecule binds to the target in addition to the scoring value. The active site of KatG in *M. tuberculosis* contains heme and nearby amino acid residues, including Tyr229, Trp107, and Met255, which together form a catalytic center. In particular, the geometry of Trp107 is critical for maintaining the catalytic activity of KatG.[10] As shown in Table 1, compound **4g**, which forms hydrogen bonds with Trp107, has the strongest anti-bacterial activity (MIC = 1 μg/mL). Compounds **4f** and **4h-m** all showed weaker antibacterial activity than **4g**, related to their failure to form hydrogen bonds with Trp107. It can therefore be speculated that the reduced anti-*Mtb* effect of compounds **3a-e** may be related to their lack of any connection with Tyr229, Trp107, and Met255 of KatG.

The structure-activity relationship (SAR) analysis is summarized in Figure 2. Comparing the MIC values of **4g** with **3a**, **4h** with **3b**, **4i** with **3c**, **4j** with **3d**, and **4k** with **3e**, respectively, it was found that the compounds whose C4 substituent was aminothiourea were more active against *Mtb* than those whose C4 substituent was 4-phenylsemicarbazide. Substitution of H on C6 or C7 of the A ring of compounds **3a-e** with F, Cl, Br, and CH3, respectively, did not improve the anti-*Mtb* activity of the compounds. However, the anti-*Mtb* activity changed with different elements or groups attached to C6 on the A ring of compounds **4f**, **4h-l**, with the following order of anti-*Mtb* contribution: CH_3 > Br = Cl > F = H > OH. Compound **4g**, with the C7 position of the A ring substituted by Br, showed the strongest anti-*Mtb* activity. We speculate that replacing H on C6 position of compound **4g** with Me may further enhance the anti-*Mtb* activity of **4g**.

Table 1. The MIC values of 13 compounds against *M. tuberculosis* and molecular docking scores with *Mtb* KatG

Comp.	Structure	MIC (μg/mL)	Lib Dock Score	Interacting animo acids
4g	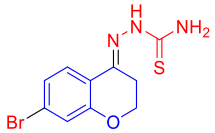	1	111.913	Hydrogen Bond: **Trp107**, Arg104 Pi-Alkyl: **Tyr229**, Val230, Ile228, His108
4k	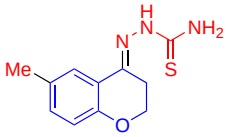	2	101.704	Hydrogen Bond: **Tyr229**, Val230, Asp137, Arg104 Pi-Pi Stacked: Hem1500 Pi-Alkyl: His108 Pi-Sulfur: **Trp107**
4f	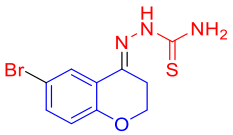	4	102.238	Hydrogen Bond: **Tyr229**, Val230, Asp137, Arg104 Pi-Pi Stacked: Hem1500 Pi-Alkyl: His108 Pi-Sulfur: **Trp107**

4j	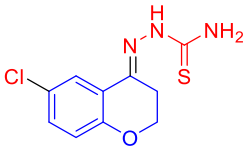	4	101.993	Hydrogen Bond: **Tyr229**, Val230, Asp137, Arg104 Pi-Pi Stacked: Hem1500 Pi-Alkyl: His108 Pi-Sulfur: **Trp107**
4i	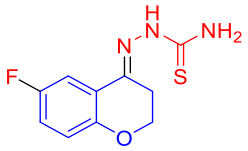	8	102.313	Hydrogen Bond: **Tyr229**, Val230, Asp137 Pi-Pi Stacked: Hem1500 Pi-Alkyl: His108, Arg104 Pi-Sulfur: **Trp107**
4h	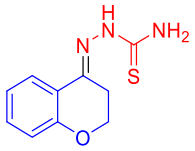	8	112.102	Hydrogen Bond: Arg104 Pi-Sigma: Hem1500 Pi-Alkyl: **Trp107**, Ile228 Pi-Cation: His108
4m	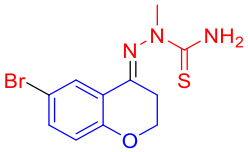	8	95.3294	Hydrogen Bond: His108, Asp137 Alkyl: Leu227, Pro232, Ala139, Hem1500 Pi-Sulfur: **Trp107**
4l	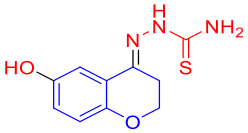	16	104.716	Hydrogen Bond: **Tyr229**, Ser315 Pi-Pi Stacked: Hem1500 Pi-Alkyl: His108, Ile228 Pi-Anion: Asp137
3a	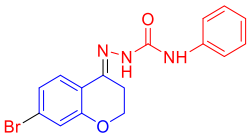	32	127.704	Hydrogen Bond: His108 Pi-Pi Stacked: Hem1500 Pi-Alkyl: Ala139 Pi-Anion: Asp137 Pi-Sigma: Ile228 Carbon Hydrogen Bond: Pro136
3b	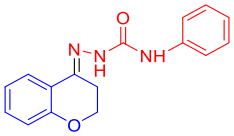	32	129.983	Hydrogen Bond: His108 Pi-Pi Stacked: Hem1500 Pi-Alkyl: Ala139 Pi-Anion: Asp137 Pi-Sigma: Ile228 Carbon Hydrogen Bond: Pro136
3c	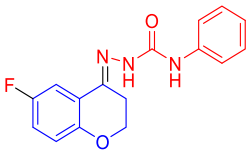	32	131.267	Hydrogen Bond: His108 Pi-Pi Stacked: Hem1500 Pi-Alkyl: Ala139 Pi-Sigma: Ile228 Carbon Hydrogen Bond: Pro136
3d	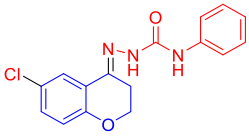	32	121.216	Hydrogen Bond: His108 Pi-Pi Stacked: Hem1500 Pi-Alkyl: Ala139, Leu227, Leu205 Pi-Sigma: Ile228 Pi-Anion: Asp137 Carbon Hydrogen Bond: Pro136
3e	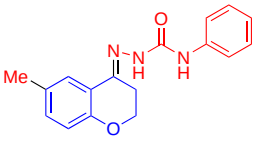	32	131.864	Hydrogen Bond: His108 Pi-Pi Stacked: Hem1500 Pi-Alkyl: Ala139, Leu227, Pro232 Pi-Sigma: Ile228 Pi-Anion: Asp137 Carbon Hydrogen Bond: Pro136

INH	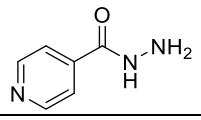	0.25	99.9806	Hydrogen Bond: **Trp107**, **Tyr229**, Val230 Pi-Sigma: Ile228 Pi-Anion: Asp137, His108, Hem1500

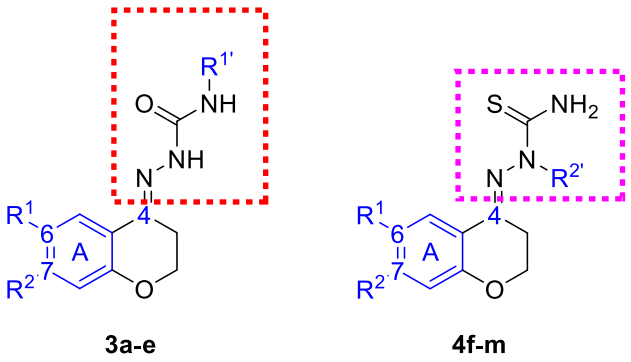

Figure 2. SAR study

Time-killing curve

Infections caused by sensitive *Mtb* typically require continuous medication for six months, while those caused by drug-resistant *Mtb* usually require longer treatment. Shortening the duration of treatment is a challenge for TB treatment. There is a need to develop drugs that can kill *Mtb* rapidly. Compound **4g** not only has a strong anti-*Mtb* effect, but as seen in Figure 3, the compound also has a desirable bactericidal effect. Isoniazid (INH) kills most *Mtb* within 24 h at the concentration of 4 MIC. However, there is a clear inflection point in the time-killing curve of isoniazid. It was obvious that isoniazid failed to kill a very small subpopulation of phenotypically drug-resistant *Mtb* even after 96 h. Interestingly, compound **4g** killed all subpopulation of *Mtb* at both 4 MIC and 2 MIC. This provides an opportunity to shorten the duration of TB treatment. Of course, whether compound **4g** can shorten the duration of TB treatment needs to be confirmed by animal infection models.

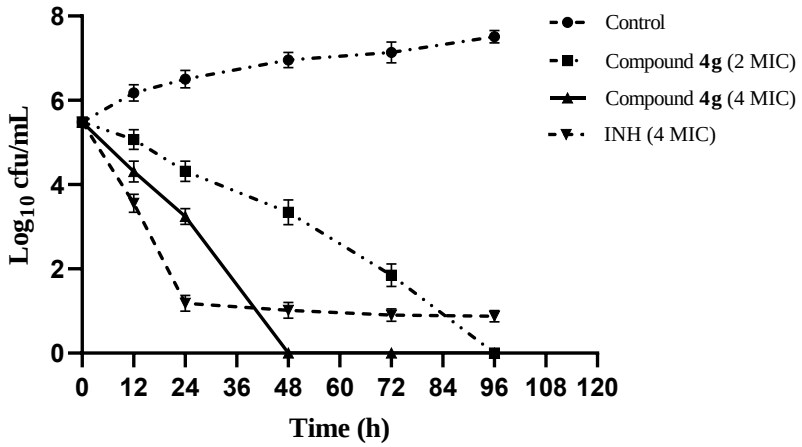

Figure 3. Time-killing curve of compound **4g**

Enzyme inhibition activity

Mtb uses KatG to keep intracellular ROS in equilibrium, and inhibition of KatG will result in intracellular ROS accumulation. Therefore, KatG may become a target for developing novel anti-*Mtb* drugs.[11] Figure 4 shows that compound **4g** has inhibitory activity against KatG of *Mtb*. The activity of KatG gradually decreased with increasing concentration of compound **4g**. Molecular docking results (Table 1) suggest that compound **4g** binds tightly to the KatG of *M. tuberculosis*, forming a hydrogen bond with Trp107 in the enzyme's active site. Apparently, the inhibitory effect of compound **4g** on KatG initially verified the prediction made by molecular docking.

Interestingly, pyrazinamide (PZA) also has the ability to inhibit the katG of *Mtb*. PZA is a first line anti-tubercular drug for which the mechanism of action remains unresolved.[12] Whether the mechanism of action of PZA is related to the inhibition of KatG enzyme needs to be further investigated.

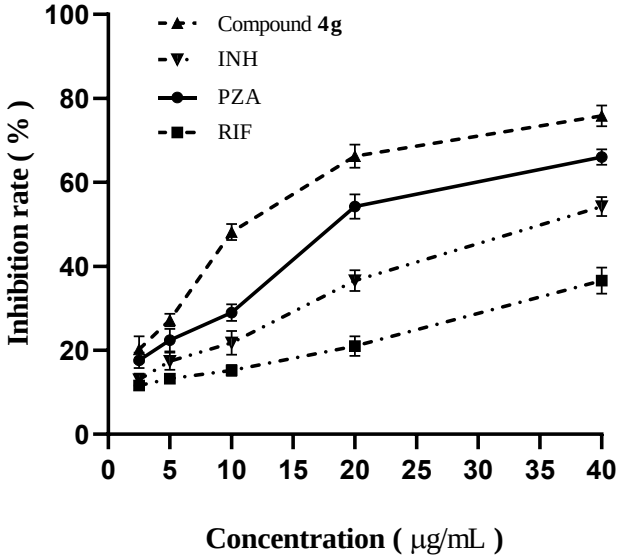

Figure 4. KatG enzyme inhibition assay

ROS measurement

We speculate that the inhibition of KatG enzyme activity in *Mtb* by compound **4g** results in the accumulation of ROS in the cells. The fluorescent probe 2',7'-dichlorofluorescin diacetate (DCFH-DA) was used to measure ROS in *Mtb* cells, where fluorescence intensity is positively correlated with the amount of ROS in the cells. Results (Figure 5, **a**) show that the concentration of compound **4g** has a dose-response relationship with the amount of ROS in the cells, which further confirms that the anti-*Mtb* activity of compound **4g** is related to its inhibition of KatG. PZA was used as reference drug, and it was observed that it can also cause the accumulation of ROS in *Mtb* cells (Figure 5, **b**), which may be related to its inhibition of KatG.

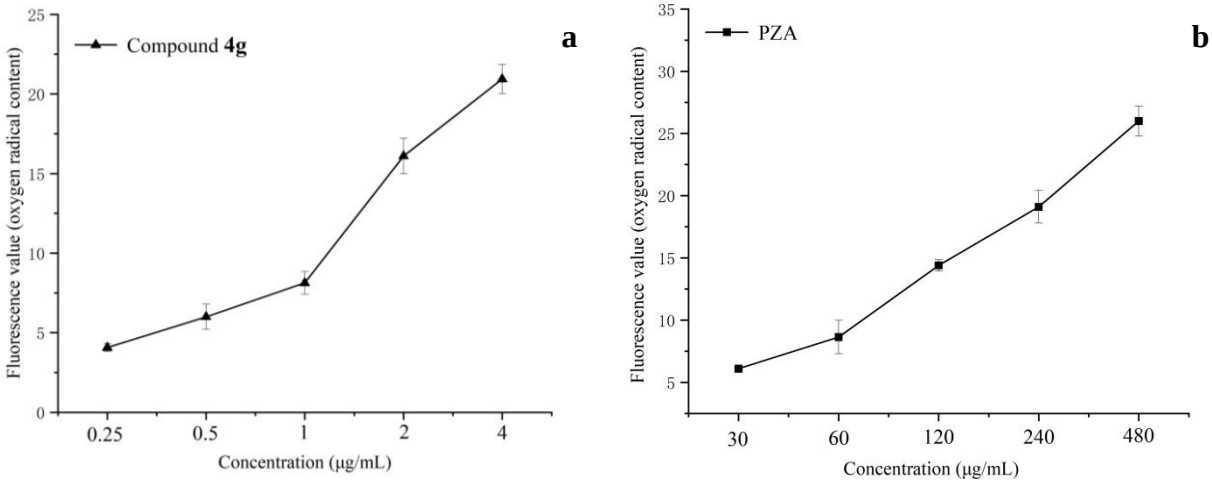

Figure 5. Intracellular ROS production of *M. tuberculosis* that treated with compound **4g** and PZA. The ROS levels of the *M. tuberculosis* was represented by the fluorescence intensity of 2',7'-dichlorofluorescein（DCF), detected by a microplate reader. **a**: indicated compound **4g**, **b**: indicated PZA.

Cytotoxicity

The cytotoxicity of compound **4g** on *Vero* cell line was evaluated using MTT assay. As shown in Table 2, compared with isoniazid, compound **4g** had a slight interference with the growth of *Vero* cells. It is generally considered safe for chemotherapy drugs to have a selective index (SI) ≥ 10. The higher the SI, the safer the compound.[13] The SI of compound **4g** was more than 10, indicating that it had no toxic effect on animal cells.

Table 2. Cytotoxicity on *Vero* cells of compound **4g**

Compound	IC_{50} (μg/mL)[a]	Selectivity index (SI)[b]
Compound **4g**	74.24 ± 2.43	74
Isoniazid	72.88 ± 1.23	292

[a] The data represent the mean ± standard deviation of three independent experiments.

[b] SI = IC_{50}/MIC.

CONCLUSIONS

The discovery of novel anti-*Mtb* drugs with novel mechanisms of action is an effective approach to tackle the challenge of drug-resistant tuberculosis. The mycobacterial enzyme KatG is a key enzyme responsible for clearing intracellular ROS. Inhibiting the activity of KatG will lead to the accumulation of ROS and the destruction of the macromolecular structure of *Mycobacterium tuberculosis*, ultimately resulting in

bacterial death.

In this study, 20 compounds were designed and 13 of them were found to have affinity with *Mtb* KatG by molecular docking. These 13 compounds were successfully synthesized by a simple method. *In vitro* antimicrobial susceptibility tests have shown that these compounds have anti-*Mtb* activity (MIC = 1-32 μg/mL). The results show that it is feasible to design anti-*Mtb* molecules by a molecular docking approach based on *Mtb* KatG.

Among the 13 compounds, compound **4g** showed the strongest anti-*Mtb* activity with an MIC of 1 μg/mL. Molecule docking exhibited that compound **4g** had a good affinity for KatG and formed a hydrogen bond with Trp107 of the active site. The experiment indicated that compound **4g** had inhibitory activity against KatG enzyme in a dose-response manner. In addition, *M. tuberculosis* showed intracellular accumulation of ROS after treatment with compound **4g**. Therefore, it can be concluded that the anti-*Mycobacterium tuberculosis* effect of compound **4g** may be related to its inhibition of KatG enzyme. However, whether the target of compound **4g** is *Mtb* KatG needs to be verified by co-crystallization data of compound **4g** with KatG.

In summary, this study provides a new idea for the development of novel anti-*Mtb* drugs. In our future work, we plan to continue to target *Mtb* KatG and design compounds with higher affinity and simultaneously form hydrogen bonds with Trp107 of KatG. These follow-up studies may lead to the discovery of novel lead compounds. The related work is in progress.

EXPERIMENTAL

Compound design

KatG is a bifunctional enzyme of *Mycobacterium tuberculosis,* consisting of a homodimer of 80 kDa subunits, both of which bind to heme.[14] The KatG enzyme reduces toxic H_2O_2 to water and molecular oxygen, mediated by the triresidue (Met-Tyr-Trp) adduct on the distal site of the heme pocket of KatG.[15]

In this study, the ligand consists of 20 compounds, which are formed by a stitching of chroman-4-one derivatives and thiosemicarbazide derivatives. As shown in Figure S1, of the 20 compounds designed (**a**-**t**), **a**-**e** were assembled from chroman-4-one derivatives with 4-phenylthiourea, **f**-**l** were assembled from chroman-4-one derivatives with aminothiourea, **m**-**r** were assembled from chroman-4-one derivatives with 2-methylthiosemicarbazide, and **s**-**t** were assembled from chroman-4-one derivatives with 4,4-dimethylthiosemicarbazide.

The crystal structure of *Mtb* KatG (PDB: 1SJ2) was obtained from the Protein Data Bank (https://www.rcsb.org) and prepared as the receptor in Discovery Studio by removing water and ligand, adding hydrogens, and minimizing energy. The 2D structures of the compounds were prepared using ChemDraw, and then energy minimization was performed using the MM2 module in ChemDraw 3D,

followed by saving the files as mol2 format. The molecular docking was carried out using Discovery Studio, and the results were analyzed visually.[16] Compounds with molecular docking scores ≥ 95 were selected for the next step of synthesis.

Materials and methods

All reactions were monitored by TLC using pre-coated aluminium plates. The ^{1}H NMR and ^{13}C NMR spectra were recorded on a Bruker ACF-400 spectrometer with tetramethylsilane (TMS) as an internal standard and DMSO-d_6 as solvent, with chemical shifts reported in δ values. The compounds were analyzed by electrospray ionization (ESI) mass spectrometry, and their *m/z* values corresponding to their accurate masses. Melting points were measured in X-4X digital display micro melting point analyzer (uncorrected, Shanghai Microelectronics Technology Co., Ltd.). FT-IR was recorded in a Shimadzu FT-IR-8400S spectrometer as KBr pellets. The high-resolution mass spectrometer (HRMS) was tested in Waters Xevo G2-S QTOF. All materials and reagents used for synthesis and analysis were commercially available and were of analytical grade and used without further purification.

The synthesis of compounds 3a-e and 4f-m

Thirteen compounds were synthesized on route outlined in Scheme 1. Dissolve 7-bromochroman-4-one (113.53 mg, 0.5 mmol) in anhydrous MeOH (6 mL) and heat reflux for 15 min until the reactants are completely dissolved. Then, *N*-phenylhydrazinecarboxamide (151.17 mg, 1 mmol) and *p*-toluenesulfonic acid (13 mg, 0.074 mmol) were added to the reaction mixture. The reaction mixture was heated and refluxed for 7 h to produce solids, then filtered, washed with MeOH, and dried to obtain compound **3a**. Using a similar synthetic route and different reaction materials, target compounds **3b-e** and **4f-m** were obtained.

(2*E*)-2-(7-Bromochroman-4-ylidene)-*N*-phenylhydrazinecarboxamide (3a)

White solid; yield 72%; mp: 246.5-248.4 ℃; ^{1}H NMR (400 MHz, DMSO-d_6): δ 9.94 (s, 1H), 8.99 (s, 1H), 8.27 (d, *J* = 8.3 Hz, 1H), 7.64 (dd, *J* = 7.8, 1.3 Hz, 2H), 7.35 – 7.25 (m, 2H), 7.16 (d, *J* = 8.0 Hz, 2H), 7.04 (t, *J* = 7.4 Hz, 1H), 4.27 (t, *J* = 6.1 Hz, 2H), 2.85 (t, *J* = 6.2 Hz, 2H). ^{13}C NMR (101 MHz, DMSO-d_6): δ 157.63, 153.92, 139.98, 139.41, 128.92, 127.71, 124.63, 123.30, 123.12, 120.69, 120.51, 120.36, 65.37, 25.47. MS (ESI): *m/z* 360.15 $[M+H]^+$. FT-IR (KBr, ν cm^{-1}): 3391, 3202 (stretch N-H), 3108 (stretch C-H Ar.), 2898 (stretch C-H), 1677 (stretch C=O), 1531 (stretch C=N), 1447 (bending N-H), 1211, 1144, 1037 (stretch C-O, C-N). ESI-HRMS $C_{16}H_{14}BrN_3O_2$ ($[M+Na]^+$): calcd 382.0162, found 382.0160.

(2*E*)-2-(Chroman-4-ylidene)-*N*-phenylhydrazinecarboxamide (3b)

White solid; yield 66%; mp: 251.3-252.6 ℃; ^{1}H NMR (400 MHz, DMSO-d_6): δ 9.87 (s, 1H), 8.94 (s, 1H), 8.30 (dd, *J* = 8.0, 1.6 Hz, 1H), 7.69 – 7.62 (m, 2H), 7.36 – 7.24 (m, 3H), 7.08 – 6.95 (m, 2H), 6.90 (dd, *J* = 8.3, 1.1 Hz, 1H), 4.25 (t, *J* = 6.1 Hz, 2H), 2.85 (t, *J* = 6.2 Hz, 2H). ^{13}C NMR (101 MHz, DMSO-d_6): δ

157.04, 153.99, 141.02, 139.44, 131.01, 128.94, 125.83, 123.05, 121.63, 120.99, 120.52, 117.66, 64.98, 25.81. MS (ESI): *m/z* 282.27 $[M+H]^+$. FT-IR (KBr, ν cm^{-1}): 3382, 3211 (stretch N-H), 3104 (stretch C-H Ar.), 2980 (stretch C-H), 1674 (stretch C=O), 1536 (stretch C=N), 1446 (bending N-H), 1215, 1138, 1045 (stretch C-O, C-N). ESI-HRMS $C_{16}H_{15}N_3O_2$ ($[M+Na]^+$): calcd 304.1056, found 304.1059.

(2*E*)-2-(6-Fluorochroman-4-ylidene)-*N*-phenylhydrazinecarboxamide (3c)

Light pink solid; yield 68%; mp: 258.3-260.1 ℃; ^{1}H NMR (400 MHz, DMSO-d_6): δ 9.92 (s, 1H), 9.05 (s, 1H), 8.20 (dd, *J* = 10.1, 3.2 Hz, 1H), 7.65 (dd, *J* = 8.6, 1.3 Hz, 2H), 7.37 – 7.27 (m, 2H), 7.17 – 7.01 (m, 2H), 6.93 (dd, *J* = 9.0, 4.8 Hz, 1H), 4.23 (t, *J* = 6.2 Hz, 2H), 2.83 (t, *J* = 6.2 Hz, 2H). ^{13}C NMR (101 MHz, DMSO-d_6): δ 158.57, 156.23, 153.99, 153.39, 140.11, 140.09, 139.36, 128.85, 123.25, 122.24, 122.16, 121.19, 119.26, 119.18, 118.07, 117.83, 111.40, 111.16, 65.14, 25.54. MS (ESI): *m/z* 300.28 $[M+H]^+$. FT-IR (KBr, ν cm^{-1}): 3383, 3196 (stretch N-H), 3099 (stretch C-H Ar.), 2986 (stretch C-H), 1676 (stretch C=O), 1537 (stretch C=N), 1439 (bending N-H), 1299, 1141, 1035 (stretch C-O, C-N). ESI-HRMS $C_{16}H_{14}FN_3O_2$ ($[M+Na]^+$): calcd 322.0962, found 322.0950.

(2*E*)-2-(6-Chlorochroman-4-ylidene)-*N*-phenylhydrazinecarboxamide (3d)

White solid; yield 91%; mp: 267.8-269.2 ℃; ^{1}H NMR (400 MHz, DMSO-d_6): δ 9.91 (s, 1H), 9.10 (s, 1H), 8.38 (d, *J* = 2.6 Hz, 1H), 7.68 – 7.60 (m, 2H), 7.37 – 7.26 (m, 3H), 7.05 (tt, *J* = 7.3, 1.2 Hz, 1H), 6.94 (d, *J* = 8.8 Hz, 1H), 4.25 (t, *J* = 6.1 Hz, 2H), 2.84 (t, *J* = 6.2 Hz, 2H). ^{13}C NMR (101 MHz, DMSO-d_6): δ 155.70, 153.99, 139.69, 139.40, 130.57, 128.88, 125.94, 124.96, 123.25, 122.63, 121.21, 119.66, 65.13, 25.41. MS (ESI): *m/z* 316.3 $[M+H]^+$. FT-IR (KBr, ν cm^{-1}): 3384, 3198 (stretch N-H), 3101 (stretch C-H Ar.), 2878 (stretch C-H), 1677 (stretch C=O), 1538 (stretch C=N), 1448 (bending N-H), 1297, 1145, 1088 (stretch C-O, C-N). ESI-HRMS $C_{16}H_{14}ClN_3O_2$ ($[M+Na]^+$): calcd 338.0667, found 338.0664.

(2*E*)-2-(6-Methylchroman-4-ylidene)-*N*-phenylhydrazinecarboxamide (3e)

White solid; yield 99%; mp: 247.3-249.6 ℃; ^{1}H NMR (400 MHz, DMSO-d_6): δ 9.82 (s, 1H), 8.92 (s, 1H), 8.07 (d, *J* = 2.2 Hz, 1H), 7.69 – 7.61 (m, 2H), 7.32 (dd, *J* = 8.5, 7.3 Hz, 2H), 7.12 – 6.98 (m, 2H), 6.79 (d, *J* = 8.3 Hz, 1H), 4.20 (t, *J* = 6.1 Hz, 2H), 2.82 (t, *J* = 6.2 Hz, 2H), 2.30 (s, 3H). ^{13}C NMR (101 MHz, DMSO-d_6): δ 155.08, 153.98, 141.25, 139.46, 131.82, 130.44, 128.95, 125.42, 123.07, 120.62, 120.55, 117.46, 64.93, 25.87, 20.76. MS (ESI): *m/z* 296.4 $[M+H]^+$. FT-IR (KBr, ν cm^{-1}): 3369, 3199 (stretch N-H), 3098 (stretch C-H Ar.), 2979 (stretch C-H), 1680 (stretch C=O), 1529 (stretch C=N), 1449 (bending N-H), 1229, 1215, 1127 (stretch C-O, C-N). ESI-HRMS $C_{17}H_{17}N_3O_2$ ($[M+Na]^+$): calcd 318.1213, found 318.1203.

(2*E*)-2-(6-Bromochroman-4-ylidene)hydrazinecarbothioamide (4f)[17]

Light yellow powder solid; yield 67%; mp: 231.5-232.7 ℃; ^{1}H NMR (400 MHz, DMSO-d_6): δ 10.32 (s, 1H), 8.51 (d, *J* = 2.5 Hz, 1H), 8.33 (d, *J* = 6.6 Hz, 2H), 7.41 (dd, *J* = 8.8, 2.5 Hz, 1H), 6.86 (d, *J* = 8.7 Hz, 1H), 4.22 (t, *J* = 6.2 Hz, 2H), 2.90 (t, *J* = 6.2 Hz, 2H). ^{13}C NMR (101 MHz, DMSO-d_6): δ 179.30, 156.64,

141.24, 133.85, 128.08, 122.79, 120.02, 113.83, 65.14, 25.57. MS (ESI): *m/z* 222.19 $[M+H]^+$.

(2*E*)-2-(7-Bromochroman-4-ylidene)hydrazinecarbothioamide (4g)

Yellow powdery solid; yield 68%; mp: 221.5-222.4 ℃; ^{1}H NMR (400 MHz, DMSO-d_6): δ 10.37 (s, 1H), 8.33 – 8.29 (m, 1H), 8.25 (d, *J* = 8.5 Hz, 1H), 8.14 (s, 1H), 7.16 – 7.07 (m, 2H), 4.25 (t, *J* = 6.2 Hz, 2H), 2.92 (t, *J* = 6.2 Hz, 2H). ^{13}C NMR (101 MHz, DMSO-d_6): δ 179.30, 158.14, 141.58, 127.93, 124.59, 123.90, 120.38, 120.23, 65.43, 25.66. MS (ESI): *m/z* 300.12 $[M+H]^+$. FT-IR (KBr, ν cm^{-1}): 3391 (stretch N-H), 3228, 3146 (stretch -NH_2), 2979 (stretch C-H), 1585 (stretch C=N), 1504 (bending N-H), 1292 (stretch C=S), 1208, 1067, 1043 (stretch C-O, C-N). ESI-HRMS $C_{10}H_{10}BrN_3OS$ ($[M+H]^+$): calcd 299.9801, found 299.9795.

(2*E*)-2-(Chroman-4-ylidene)hydrazinecarbothioamide (4h)[18]

White powdery solid; yield 65%; mp: 215.3-217.7 ℃; ^{1}H NMR (400 MHz, DMSO-d_6): δ 10.30 (s, 1H), 8.27 (dd, *J* = 8.0, 1.8 Hz, 2H), 8.06 (s, 1H), 7.28 (ddd, *J* = 8.5, 7.1, 1.7 Hz, 1H), 6.97 – 6.86 (m, 2H), 4.22 (t, *J* = 6.2 Hz, 2H), 2.91 (t, *J* = 6.2 Hz, 2H). ^{13}C NMR (101 MHz, DMSO-d_6): δ 179.23, 157.58, 142.71, 131.49, 126.07, 121.56, 120.70, 117.67, 65.03, 25.97. MS (ESI): *m/z* 222.3 $[M+H]^+$.

(2*E*)-2-(6-Fluorochroman-4-ylidene)hydrazinecarbothioamide (4i)

Light yellow powdery solid; yield 65%; mp: 226.8-228.3 ℃; ^{1}H NMR (400 MHz, DMSO-d_6): δ 10.33 (s, 1H), 8.30 (d, *J* = 11.4 Hz, 2H), 8.18 (dd, *J* = 10.2, 3.2 Hz, 1H), 7.12 (td, *J* = 8.5, 3.2 Hz, 1H), 6.91 (dd, *J* = 9.0, 4.8 Hz, 1H), 4.20 (t, *J* = 6.2 Hz, 2H), 2.89 (t, *J* = 6.2 Hz, 2H). ^{13}C NMR (101 MHz, DMSO-d_6): δ 179.32, 158.56, 156.22, 153.93, 141.61, 141.59, 121.97, 121.88, 119.27, 119.19, 118.59, 118.35, 111.58, 111.34, 65.21, 25.69. MS (ESI): *m/z* 240.2 $[M+H]^+$. FT-IR (KBr, ν cm^{-1}): 3426 (stretch N-H), 3188, 3132 (stretch -NH_2), 2976 (stretch C-H), 1590 (stretch C=N), 1501 (bending N-H), 1282 (stretch C=S), 1169, 1093, 1044 (stretch C-O, C-N). ESI-HRMS $C_{10}H_{10}FN_3OS$ ($[M+H]^+$): calcd 240.0601, found 240.0593.

(2*E*)-2-(6-Chlorochroman-4-ylidene)hydrazinecarbothioamide (4j)[18]

White powdered solid; yield 60%; mp: 238.5-239.6 ℃; ^{1}H NMR (400 MHz, DMSO-d_6): δ 10.33 (s, 1H), 8.42 – 8.24 (m, 3H), 7.29 (dd, *J* = 8.8, 2.7 Hz, 1H), 6.91 (d, *J* = 8.8 Hz, 1H), 4.22 (t, *J* = 6.2 Hz, 2H), 2.90 (t, *J* = 6.2 Hz, 2H). ^{13}C NMR (101 MHz, DMSO-d_6): δ 179.32, 156.22, 141.28, 131.03, 126.02, 125.22, 122.31, 119.63, 65.18, 25.58. MS (ESI): *m/z* 253.9 $[M-H]^-$.

(2*E*)-2-(6-Methylchroman-4-ylidene)hydrazinecarbothioamide (4k)[19]

White powder solid; yield 77%; mp: 229.6-231.2 ℃; ^{1}H NMR (400 MHz, DMSO-d_6): δ 10.27 (s, 1H), 8.30 (s, 1H), 8.10 – 8.04 (m, 2H), 7.08 (dd, *J* = 8.4, 2.2 Hz, 1H), 6.77 (d, *J* = 8.3 Hz, 1H), 4.17 (t, *J* = 6.2 Hz, 2H), 2.88 (t, *J* = 6.2 Hz, 2H), 2.26 (s, 3H). ^{13}C NMR (101 MHz, DMSO-d_6): δ 179.18, 155.60, 142.85, 132.30, 130.45, 125.74, 120.23, 117.41, 65.00, 26.01, 20.61. MS (ESI): *m/z* 236.3 $[M+H]^+$.

(2*E*)-2-(6-Hydroxychroman-4-ylidene)hydrazinecarbothioamide (4l)

White powdered solid; yield 62%; mp: 232.8-234.2 ℃; ^{1}H NMR (400 MHz, DMSO-d_6): δ 10.28 (s, 1H), 8.98 (s, 1H), 8.32 – 8.20 (m, 1H), 7.95 – 7.81 (m, 1H), 7.53 (d, J = 2.6 Hz, 1H), 6.78 – 6.68 (m, 2H), 4.12 (t, J = 6.2 Hz, 2H), 2.84 (t, J = 6.2 Hz, 2H). ^{13}C NMR (101 MHz, DMSO-d_6): δ 179.23, 151.84, 150.97, 143.52, 121.02, 119.60, 118.29, 110.50, 65.01, 26.24. MS (ESI): *m/z* 235.93 $[M-H]^-$. FT-IR (KBr, ν cm^{-1}): 3444 (stretch -OH), 3323, 3297, 3178 (stretch N-H), 2907 (stretch C-H), 1591 (stretch C=N), 1493 (bending N-H), 1438 (stretch C=S), 1268, 1104, 1043 (stretch C-O, C-N). ESI-HRMS $C_{10}H_{11}N_3O_2S$ ($[M+Na]^+$): calcd 260.0464, found 260.0463.

(2*E*)-2-(6-Bromochroman-4-ylidene)-1-methylhydrazinecarbothioamide (4m)

Light yellow powder; yield 65%; mp: 197.2-198.9 ℃; ^{1}H NMR (400 MHz, DMSO-d_6): δ 8.18 (d, J = 2.5 Hz, 1H), 7.56 (dd, J = 8.8, 2.6 Hz, 1H), 6.95 (d, J = 8.8 Hz, 1H), 4.32 – 4.25 (m, 1H), 3.43 (s, 3H), 2.86 – 2.78 (m, 1H). ^{13}C NMR (101 MHz, DMSO-d_6): δ 180.57, 161.95, 157.37, 135.85, 128.80, 121.38, 120.26, 113.13, 65.50, 41.68, 27.57. MS (ESI): *m/z* 311.76 $[M-H]^-$. FT-IR (KBr, ν cm^{-1}): 3425, 3258 (stretch $-NH_2$), 3141 (stretch C-H Ar.), 2898 (stretch C-H), 1579 (stretch C=N), 1472 (bending N-H), 1358 (bending C-H), 1213 (stretch C=S), 1134, 1038 (stretch C-O, C-N). ESI-HRMS $C_{11}H_{12}BrN_3OS$ ($[M+Na]^+$): calcd 335.9777, found 335.9768.

Minimal inhibitory concentration (MIC)

The anti-*Mtb* activity of the compounds was determined by resazurin microtitre plate assay (REMA).[20] *Mtb* H_{37}Rv (ATCC 27294) was used as reference strain, and resazurin used as an oxidation–reduction indicator. The REMA plate method was performed in 7H9 broth containing of 0.1% Casitone，0.5% glycerol, oleic acid, albumin, glucose, and peroxidase (Becton-Dickinson, Sparks, MD, USA). Compounds were added to the 7H9 broth at a final concentration of 1-64 μg/mL in 96-well plates. Isoniazid was used as a positive control. Antibiotic-free growth control and sterility control without inoculation were also included. The inoculum was adjusted to McFarland 1.0 using a turbidimeter from fresh colonies on 7H11 agar, diluted 1:10 in 7H9 broth, with 100 μL as the inoculum. The plates were covered and sealed in plastic bag, and incubated at 37 ℃ in a normal atmosphere. After 7 days of incubation, 30 μL of resazurin solution was added to each well, incubated for 48 h at 37 ℃, and color development was assessed. If the blue color in the wells turns pink, it indicates that *Mtb* is growing, and MIC is defined as the minimum concentration of the compound that prevents the color change. Each set of experiments was repeated three times.

Time-killing curve

Among the 13 compounds, compound **4g** showed the strongest inhibitory activity against *Mtb* with an MIC value of 1 μg/mL. Time-killing curves were measured to further evaluate whether compound **4g**

could kill phenotypically drug-resistant bacteria. Compound **4g** was prepared in 7H9 broth as 2 μg/mL (2 MIC) and 4 μg/mL (4 MIC) solutions, respectively. Isoniazid (1 μg/mL, 4 MIC) was used as reference drug. Each tube was inoculated with 100 μL of 10^8 CFU/mL bacterial solution and incubated at 37 ℃. Samples of 100 μL were taken at 12, 24, 48, 72, and 96 h after incubation for 1:10 dilution, respectively. The diluted bacterial solution (100 μL) was applied on 7H11 solid plate and continued to incubate for 2 weeks, and the colony number was measured. Each group of experiments was repeated three times.

***In vitro* enzymatic assay**

The UV absorption values of H_2O_2 were measured by spectrophotometic method.[21] The measurement wavelength was 240 nm and the ambient temperature was 25 ± 1 ℃. The KatG enzyme was obtained from *M. tuberculosis* H_{37}Rv isolated and purified according to the literature.[22] KatG solution (1 mg/mL) was prepared with phosphate buffer. The activity unit of this enzyme solution is 10,000 U/mL. Reference drugs (isoniazid, pyrazinamide, rifampin) and compound **4g** were diluted with phosphate buffer into 2.5, 5, 10, 20, and 40 μg/mL solutions. Hydrogen peroxide (10 mM) was prepared by adding 0.1134 mL of 30% hydrogen peroxide to 100 mL of phosphate buffer. The operation procedure is shown in Table 3. The enzyme inhibition rate was calculated according to the following formula: Inhibition rate (%) = $\{1-(OD_{Standard} - OD_{Test}/OD_{Standard})\} \times 100\%$.

Table 3. The procedures for evaluating catalase activity

Reagents	Test	Standard	Blank
KatG solution	500 μL	—	—
Phosphate buffer	—	1500 μL	2500 μL
Samples (INH, RIF, PZA, and compound **4g**)	1000 μL	—	—
Mix the tube with vortex and incubate at 25 ℃ for 30 min, then add hydrogen peroxide:			
Hydrogen peroxide	1000 μL	1000 μL	—
Spin the tubes for 10 s and hold at 25 ± 1 ℃ for 2 min. Then add 1000 μL of 1.8 M sulfuric acid to stop the reaction. Record the absorbance at the reagent blank at 240 nm.			

ROS measurement

To test the effect of different concentrations of compound **4g** on the accumulation of ROS in *M. tuberculosis* cells, the final concentrations of compound **4g** in the test system were 1/4 MIC (0.25 μg/mL), 1/2 MIC (0.5 μg/mL), MIC (1 μg/mL), 2 MIC (2 μg/mL) and 4 MIC (4 μg/mL), respectively. The corresponding final concentrations of PZA were 1/4 MIC (30 μg/mL), 1/2 MIC (60 μg/mL), MIC (120 μg/mL), 2 MIC (240 μg/mL), and 4 MIC (480 μg/mL). DCFH-DA (2′,7′-dichlorofluorescein diacetate)

fluorescent probe was used to measure intracellular reactive oxygen species (ROS) levels. Mycobacterial cells (1×10^{10} CFU/mL) treated with drugs (that untreated used as negative control) were incubated under 37 ℃ for 4 h, DCFH-DA solution (5 μM) was added to the cultures and reincubated for 30 min. The mycobacterial suspension was then centrifuged, washed and resuspended in PBS buffer to remove extracellular excess DCFH-DA. The fluorescent signal (λex/λem = 484/525 nm) was measured on a fluorescence Microplate Reader (SpectraMax Gemini EM) to evaluate ROS production in mycobacteria cells.

***In vitro* cytotoxicity assays**

Cytotoxicity of compound **4g** was determined with the Vero cell line (ATCC CCL-81) using the MTT (3-(4,5-dimethyl-2-thiazolyl)-2,5-diphenyl-2*H*-tetrazolium bromide) assay as previously described.[23] The half maximal inhibitory concentration (IC_{50}) was defined as the concentration of the test sample required to inhibit the *Vero* cells viability by half. The selectivity index (SI) for the test sample was calculated by dividing the IC_{50} value with the MIC value.

ACKNOWLEDGEMENTS

This work was supported by the National Natural Science Foundation of China (82060635, 81760629, and 81460531).

The authors are grateful with Professor Qian-Jun Zhang for recording NMR and ESI-MS spectrum.

SUPPORTING INFORMATION

Additional supporting information including FigureS1, ^{1}H, ^{13}C NMR, IR and HRMS spectra of compounds may be found online in the Supporting Information section at the end of the article.

REFERENCES

1. C. Dye and B. G. Williams, *Science*, 2010, **328**, 856.
2. S. Bagcchi, *Lancet Microbe*, 2023, **4**, e20.
3. A. Natarajan, P. M. Beena, A. V. Devnikar, and S. Mali, *Indian J. Tuberc.*, 2020, **67**, 295.
4. S. T. Saengchantara and T. W. Wallace, *Nat. Prod. Rep.*, 1986, **3**, 465.
5. (a) S. K. Roy, N. Kumari, S. Gupta, S. Pahwa, H. Nandanwar, and S. M. Jachak, *Eur. J. Med. Chem.*, 2013, **66**, 499; (b) M. Mujahid, R. G. Gonnade, P. Yogeeswari, D. Sriram, and M. Muthukrishnan, *Bioorg. Med. Chem. Lett.*, 2013, **23**, 1416; (c) T. Yempala, D. Sriram, P. Yogeeswari, and S. Kantevari, *Bioorg. Med. Chem. Lett.*, 2012, **22**, 7426; (d) S. Noushini, E. Alipour, S. Emami, M. Safavi, S. K. Ardestani, A. R. Gohari, A. Shafiee, and A. Foroumadi, *Daru*, 2013, **21**, 31; (e) S. Inui, T. Hosoya, Y. Shimamura, S. Masuda, T. Ogawa, H. Kobayashi, K. Shirafuji, R. T. Moli, I. Kozone,

K. Shin-ya, and S. Kumazawa, *J. Agric. Food Chem.*, 2012, **60**, 11765; (f) T. C. McKee, H. R. Bokesch, J. L. McCormick, M. A. Rashid, D. Spielvogel, K. R. Gustafson, M. M. Alavanja, J. H. Cardelline, and M. R. Boyd, *J. Nat. Prod.*, 1997, **60**, 431.

6. (a) M. A. Bhat, A. A. Khan, H. A. Ghabbour, C. K. Quah, and H. K. Fun, *Trop. J. Pharm. Res.*, 2016, **15**, 1751; (b) H. Beraldo and D. Gambino, *Mini Rev. Med. Chem.*, 2004, **4**, 31; (c) I. Mir, M. T. Siddiqui, and A. Comrie, *Tetrahedron*, 1970, **26**, 5235; (d) M. C. Cardia, S. Distinto, E. Maccioni, A. Plumitallo, M. L. Sanna, M. Saddi, and A. Delogu, *J. Heterocycl. Chem.*, 2006, **43**, 1337.
7. (a) B. J. Kinsley, Pepys, and Sutherland, *Tubercle*, 1960, **41**, 399; (b) J. M. Belardinelli and H. R. Morbidoni, *Mol. Microbiol.*, 2012, **86**, 568; (c) A. E. Grzegorzewicz, N. Eynard, A. Quémard, E. J. North, A. Margolis, J. J. Lindenberger, V. Jones, J. Korduláková, P. J. Brennan, R. E. Lee, D. R. Ronning, M. R. McNeil, and M. Jackson, *ACS Infect. Dis.*, 2015, **1**, 91.
8. K. Ranguelova, S. Girotto, G. J. Gerfen, S. W. Yu, J. Suarez, L. Metlitsky, and R. S. Magliozzo, *J. Biol. Chem.*, 2007, **282**, 6255.
9. C. X. Liu, X. Zhao, L. Wang, and Z. C. Yang, *Microb. Pathog.*, 2022, **165**, 105507.
10. X. B. Zhao, S. W. Yu, and R. S. Magliozzo, *Biochemistry*, 2007, **46**, 3161.
11. (a) M. P. Brynildsen, J. A. Winkler, C. S. Spina, I. C. MacDonald, and J. J. Collins, *Nat. Biotechnol.*, 2013, **31**, 160; (b) T. Bertrand, N. A. Eady, J. N. Jones, Jesmin, J. M. Nagy, B. Jamart-Grégoire, E. L. Raven, and K. A. Brown, *J. Biol. Chem.*, 2004, **279**, 38991.
12. N. A. Dillon, N. D. Peterson, H. A. Feaga, K. C. Keiler, and A. D. Baughn, *Sci. Rep.*, 2017, **7**, 6135.
13. O. A. Peña-Morán, M. L. Villarreal, L. Álvarez-Berber, A. Meneses-Acosta, and V. Rodríguez-López, *Molecules*, 2016, **21**, 1013.
14. (a) K. Johnsson, W. A. Froland, and P. G. Schultz, *J. Biol. Chem.*, 1997, **272**, 2834; (b) R. S. Magliozzo and J. A. Marcinkeviciene, *J. Am. Chem. Soc.*, 1996, **118**, 11303.
15. O. J. Njuma, E. N. Ndontsa, and D. C. Goodwin, *Arch. Biochem. Biophys.*, 2014, **544**, 27.
16. Q. Wang, J. W. He, D. Wu, J. Wang, J. Yan, and H. Li, *J. Lumin.*, 2015, **164**, 81.
17. R. Siles, S. E. Chen, M. Zhou, K. G. Pinney, and M. L. Trawick, *Bioorg. Med. Chem. Lett.*, 2006, **16**, 4405.
18. J. I. Song, L. M. Jones, G. E. Chavarria, A. K. Charlton-Sevcik, A. Jantz, A. Johansen, L. Bayeh, V. Soeung, L. K. Snyder, S. D. Lade, D. J. Chaplin, M. L. Trawick, and K. G. Pinney, *Bioorg. Med. Chem. Lett.*, 2013, **23**, 2801.
19. G. Turan-Zitouni, P. Chevallet, K. Erol, and B. S. Boydağ, *Il Farmaco.*, 1997, **52**, 569.
20. J. C. Palomino, A. Martin, M. Camacho, H. Guerra, J. Swings, and F. Portaels, *Antimicrob. Agents Chemother.*, 2002, **46**, 2720.
21. R. F. Beers and I. W. Sizer, *J. Biol. Chem.*, 1952, **195**, 133.

22. J. A. Marcinkeviciene, R. S. Magliozzo, and J. S. Blanchard, *J. Biol. Chem.*, 1995, **270**, 22290.
23. M. L. Gan, L. F. Han, R. F. Wang, and Z. C. Yang, *S. Afr. J. Bot.*, 2019, **121**, 92.